Clim. Past Discuss., 11, 1437–1477, 2015
www.clim-past-discuss.net/11/1437/2015/
doi:10.5194/cpd-11-1437-2015

Climate of the Past Discussions
Open Access

Phase relationships between orbital forcing and the composition of air trapped in Antarctic ice cores

L. Bazin[1], A. Landais[1], V. Masson-Delmotte[1], C. Ritz[2], G. Picard[2], E. Capron[3], J. Jouzel[1], M. Dumont[4], M. Leuenberger[5], and F. Prié[1]

[1]Laboratoire des Sciences du Climat et de l'Environnement, UMR8212, CEA-CNRS-UVSQ, Orme des Merisiers, Gif sur Yvette, France
[2]Laboratoire de Glaciologie et Géophysique de l'Environnement, UMR 5183, Univ. Grenoble Alpes-CNRS, Grenoble, France
[3]British Antarctic Survey, NERC, Cambridge, UK
[4]Météo-France-CNRS, CNRM-GAME UMR 3589, CEN, Grenoble, France
[5]Climate and Environmental Physics, Physics Institute and Oeschger Center for Climate Change Research, University of Bern, Bern, Switzerland

Received: 9 March 2015 – Accepted: 31 March 2015 – Published: 23 April 2015

Correspondence to: L. Bazin (lucie.bazin@lsce.ipsl.fr)

Published by Copernicus Publications on behalf of the European Geosciences Union.

Abstract

Orbital tuning is central for ice core chronologies beyond annual layer counting, available back to 60 ka (i.e. thousand of years before 1950) for Greenland ice cores. While several complementary orbital tuning tools have recently been developed using $\delta^{18}O_{atm}$, $\delta O_2 / N_2$ and air content with different orbital targets, quantifying their uncertainties remains a challenge. Indeed, the exact processes linking variations of these parameters, measured in the air trapped in ice, to their orbital targets are not yet fully understood. Here, we provide new series of $\delta O_2 / N_2$ and $\delta^{18}O_{atm}$ data encompassing Marine Isotopic Stage (MIS) 5 (between 100–160 ka) and the oldest part (380–800 ka) of the East Antarctic EPICA Dome C (EDC) ice core. For the first time, the measurements over MIS 5 allow an inter-comparison of $\delta O_2 / N_2$ and $\delta^{18}O_{atm}$ records from three East Antarctic ice core sites (EDC, Vostok and Dome F). This comparison highlights a site-specific relationship between $\delta O_2 / N_2$ and its local summer solstice insolation. Such a relationship increases the uncertainty associated with the use of $\delta O_2 / N_2$ as a tool for orbital tuning. Combining records of $\delta^{18}O_{atm}$ and $\delta O_2 / N_2$ from Vostok and EDC, we evidence a loss of orbital signature for these two parameters during periods of minimum eccentricity ($\sim$ 400, $\sim$ 720–800 ka). Our dataset reveals a time-varying lag between $\delta O_2 / N_2$ and $\delta^{18}O_{atm}$ over the last 800 ka that we interpret as variations of the lag between $\delta^{18}O_{atm}$ and precession. Large lags of $\sim$ 5 ka are identified during Terminations I and II, associated with strong Heinrich events. On the opposite, minimal lags ($\sim$ 1–2 ka) are identified during four periods characterized by high eccentricity, intermediate ice volume and no Heinrich events (MIS 6–7, the end of MIS 9, MIS 15 and MIS 17). We therefore suggest that the occurrence of Heinrich events influences the response of $\delta^{18}O_{atm}$ to precession.

CPD
11, 1437–1477, 2015

1 Introduction

Past changes in climate and atmospheric composition are recorded in a variety of ice core proxies. The EPICA Dome C (EDC) ice core has provided the longest available records, and documented glacial–interglacial changes in atmospheric greenhouse gases concentrations (Spahni et al., 2005; Loulergue et al., 2008; Lüthi et al., 2008) and Antarctic temperature (Jouzel et al., 2007) back to 800 ka (thousands of years before present, present being AD 1950). Precise and coherent ice core chronologies are critical to establish the sequence of events and to understand these past changes. A specificity of ice core chronologies lies in the requirement to calculate ice and gas chronologies, due to the fact that air is trapped several tens of meters below the ice sheet surface. The depth at which this trapping process occurs is called the lock-in depth (LID).

Ice core age scales are usually constructed using ice flow models and different age constraints (Parrenin et al., 2001, 2004, 2007; Buiron et al., 2011). Lemieux-Dudon et al. (2010) have developed a new dating tool (Datice) allowing for the first time to produce an optimized and common chronology for several ice cores from Antarctica and Greenland, over the past 50 ka. Using an improved version of this dating tool, as well as an extended set of age constraints, Bazin et al. (2013) and Veres et al. (2013) have established a common chronology (AICC2012 chronology) for four Antarctic ice cores (Vostok; EDC; EPICA Dronning Maud Land, EDML; Talos Dome ice core, TALDICE) and one Greenland ice core (NorthGRIP, NGRIP) extending back to 800 ka for EDC. A key limitation in deep ice core chronologies lies in the lack of absolute age constraints prior to layer counting in NGRIP (for ages older than 60 ka, Svensson et al., 2008). Orbital tuning of several parameters measured in the air trapped in ice cores (air content, $\delta O_2/N_2$ and $\delta^{18}O_{atm}$) has thus played a central role for the construction of the AICC2012 chronology. Orbital tuning permits to attribute ages deduced from the integrated summer insolation, summer insolation or precession variations to their ob-

CPD
11, 1437–1477, 2015

served counterparts in air content, $\delta O_2/N_2$ or $\delta^{18}O_{atm}$ respectively, with acceptable uncertainties.

Orbital tuning is commonly applied to deep sea cores, using the orbital properties of benthic foraminifera ^{18}O records, themselves related to changes in ice volume (Imbrie and Imbrie, 1980). The most closely related ice core parameter is $\delta^{18}O_{atm}$, ^{18}O of atmospheric O_2. Ice core records of $\delta^{18}O_{atm}$ are strongly correlated with variations of insolation in the precession band, with a lag assumed to be $\sim$ 5–6 ka as established for the last termination (glacial–interglacial transition, Bender et al., 1994; Jouzel et al., 1996; Petit et al., 1999; Shackleton et al., 2000; Dreyfus et al., 2007). The modulation of precession on $\delta^{18}O_{atm}$ operates through the biosphere productivity and changes in low latitude water cycle (Bender et al., 1994; Malaizé et al., 1999; Wang et al., 2008; Severinghaus et al., 2009; Landais et al., 2007, 2010). The significant time delay between precession and $\delta^{18}O_{atm}$ is not straightforward to explain. It partly depends on the 1–2 ka residence time of O_2 in the atmosphere and on the complex response of biosphere productivity and tropical water cycle to precession changes. Caley et al. (2011) have shown lags of several thousand years between the responses of Indian and Asian monsoon systems to orbital forcing over the last 40 ka. Moreover, variations of $\delta^{18}O_{atm}$ are not only affected by the response to orbital forcing, but also by the millennial climate variability (Severinghaus et al., 2009; Landais et al., 2007). During Terminations I and II, $\delta^{18}O_{atm}$ maxima have been linked to Heinrich stadials 1 and 11 (Landais et al., 2013). Because of these complex interactions, the lag between $\delta^{18}O_{atm}$ and precession should vary with time (Leuenberger, 1997; Jouzel et al., 2002). However, for dating purposes, this lag has been assumed to be constant with an uncertainty of a quarter of a precession cycle (6 ka; Parrenin et al., 2007; Dreyfus et al., 2007).

Two other ice core parameters have been used for orbital tuning, but with a completely different underlying mechanism. The air content and $\delta O_2/N_2$ measured in the air trapped in ice cores are controlled by the enclosure process near the close-off depth (depth of closure of ice interstices and formation of air bubbles). At this depth, a depletion of the ratio O_2/N_2 compared to the atmospheric ratio is observed and attributed to

CPD
11, 1437–1477, 2015

the smaller size of O_2 molecules compared to N_2 ones (Battle et al., 1996; Huber et al., 2006; Severinghaus and Battle, 2006). It is expected that the entrapment process and the associated O_2 effusion effect are linked to the physical properties of snow at this depth. Because snow metamorphism is very strong at the surface of the ice sheet in summer (Town et al., 2008; Picard et al., 2012), snow physical properties are expected to be driven by local summer insolation. Records of $\delta O_2/N_2$ and air content measured at Vostok, Dome F and EDC indeed depict variability at orbital frequencies, which appears in phase with local summer insolation (Bender, 2002; Kawamura et al., 2007; Raynaud et al., 2007; Lipenkov et al., 2011; Landais et al., 2012).

In summary, $\delta^{18}O_{atm}$ provides a relationship between the gas phase age and orbital forcing, due to changes in atmospheric composition driven by changes in low latitude hydrological cycle and biosphere productivity. Air content and $\delta O_2/N_2$ provide a relationship between the ice phase age and local insolation, due to the impact of snow metamorphism on air trapping processes.

$\delta^{18}O_{atm}$ is a well-mixed atmospheric signal, allowing synchronization of different ice core records. It also has a potential to link ice cores with climate records from other latitudes (e.g. global ice volume, low latitude hydrological cycle and biosphere productivity). However, due to the numerous and complex processes affecting the $\delta^{18}O_{atm}$, this orbital dating tool is generally associated with an uncertainty of 6 ka, namely a quarter of a precession cycle. An important challenge to progress on chronological issues is to estimate the variations of the lag between $\delta^{18}O_{atm}$ and precession over the last eight glacial–interglacial cycles.

Contrary to $\delta^{18}O_{atm}$, $\delta O_2/N_2$ and air content are not influenced by remote climatic-driven signals such as low latitude hydrological cycle or Northern Hemisphere land ice volume. However, local climate effects on firn pore structure are not fully understood. If solar radiations impact on $\delta O_2/N_2$ and air content as suspected, it occurs through surface snow metamorphism. Therefore, it depends on the surface energy budget, snow albedo, and upper snow temperature gradients (Picard et al., 2012). However, strong modifications of layering and microstructure are also observed at several tenths

CPD
11, 1437–1477, 2015

of meters below the surface (Hörhold et al., 2012). It is therefore expected that pore structure at close-off is also affected by changes in dust load (Freitag et al., 2013) and/or accumulation rates (Hutterli et al., 2010). The direct link originally assumed between summer solstice insolation and $\delta O_2/N_2$ variations is therefore complicated by these different influences impacting on firnification.

These different limitations for each parameter have recently motivated a first assessment of the coherency between the different orbital dating tools in ice cores. Indeed, in the framework of the AICC2012 chronology construction (Bazin et al., 2013), we took advantage of available records of $\delta O_2/N_2$, air content and $\delta^{18}O_{atm}$ over the period 100–400 ka from the Vostok ice core (Petit et al., 1999; Bender, 2002; Suwa and Bender, 2008b; Lipenkov et al., 2011). We showed that the final chronology was the same using one or the other orbital markers with uncertainties of up to 7, 4 and 6 ka were attributed to air content, $\delta O_2/N_2$ and $\delta^{18}O_{atm}$, respectively. However, this first assessment was restricted to one single ice core covering only the last 400 ka. The large uncertainties associated with the different orbital markers in this case were partly due to the low resolution of the existing records and to the poor quality of the $\delta O_2/N_2$ data affected by gas loss (Landais et al., 2012). Gas loss, which occurs through micro-cracks during coring and ice core storage at warm temperature (typically freezers at −25 °C), favours the loss of O_2, and alters the original $\delta O_2/N_2$ signal (Kawamura et al., 2007; Bender et al., 1995). In this case, drifts in $\delta O_2/N_2$ have been shown to be related to storage duration (Kawamura et al., 2007) and must be corrected prior to the use of the data.

Our current understanding of these dating tools motivates further comparison of $\delta O_2/N_2$ and $\delta^{18}O_{atm}$ records, obtained (i) at high temporal resolution, (ii) from different East Antarctic ice cores, (iii) under different orbital and climatic contexts and (iv) on ice stored at very cold temperature (−50 °C) to avoid gas loss correction. In order to complement existing records from the Vostok and Dome F ice cores, we have performed new measurements on the long EDC ice core, for which only parts of the

CPD
11, 1437–1477, 2015

$\delta O_2/N_2$ record were obtained from samples of well-conserved ice (−50 °C) (Landais et al., 2012).

Our goal is to assess the robustness of the use of $\delta O_2/N_2$ and $\delta^{18}O_{atm}$ as combined dating tools over the last 800 ka. For this purpose, we have performed new measurements of $\delta^{18}O_{atm}$ and $\delta O_2/N_2$ on ice stored at −50 °C (i.e. non-affected by gas loss) on the EDC ice core over Marine Isotope Stage (MIS) 5 and between 380–800 ka. Section 2 describes the new measurements from the EDC ice core complementing earlier data (Dreyfus et al., 2007, 2008; Landais et al., 2012, 2013; Bazin et al., 2013). Section 3 is dedicated to the analyses of the datasets, the inter-comparison of Vostok, Dome F and EDC data over MIS 5, as well as an investigation of the lags between $\delta O_2/N_2$ and $\delta^{18}O_{atm}$ during the past 800 ka and their implications for orbital tuning. These records enable us to check the coherency of these parameters for orbital tuning and to provide recommendation for their use in ice core chronologies.

2 Analytical method and measurements

The isotopic composition measurements of air trapped in well-conserved ice from EDC were performed at LSCE. The samples were cut in Antarctica in the archive trench at −40 °C maximum, and then kept at −50 °C during transportation and storage. Measurements were performed only a few months after their transportation from Antarctica. To prevent any contamination from exchanges with ambient air due to micro-cracks, we shave off 3–5 mm of ice on each face, and the air is extracted from a sample of ∼ 10 g of ice. Two different extraction methods have been used, either a manual or a semi-automatic line.

The manual method consists of a melt-refreeze technique (Sowers et al., 1989; Landais et al., 2003) for extracting the air trapped in the ice samples. The sample is placed in a cold flask and then the air in the flask is pumped. The trapped air is extracted by melting and refreezing the sample and is then cryogenically transferred in a stainless-steel tube immersed in liquid helium.

CPD
11, 1437–1477, 2015

For the semi-automatic extraction line, we proceed with two exterior air samples and three ice samples with duplicates each day. The samples are placed in cold flasks and the air in the flasks is pumped; the air trapped in ice is extracted by melting of the samples and left at room temperature during one hour minimum. The air samples are then transferred one at a time through CO_2 and water vapour traps before being cryogenically trapped into a manifold immersed in liquid helium. An inter-comparison of the two extraction lines has been conducted using air extracted from NGRIP ice samples. No bias is observed in-between the two analytical extraction methods.

After a waiting time of 40 min, allowing the tubes to reach room temperature, measurements are performed with a dual inlet Delta V plus (Thermo Electron Corporation) mass spectrometer. A classical run is composed of 16 measurements of the sample in parallel with 16 measurements of a standard of dried exterior air. We simultaneously measure ^{18}O, $\delta O_2/N_2$ and ^{15}N. The data are then calibrated against the mean exterior air values and corrected for mass interferences following the standard methodologies (Severinghaus et al., 2001; Landais et al., 2003).

We were able to replicate 108 samples over 145 depth levels due to the small size of samples. The $\delta O_2/N_2$ and ^{18}O measurements are corrected for gravitational fractionation using the following equations:

$$\delta^{18}O_{atm} = \delta^{18}O - 2 \cdot \delta^{15}N \quad (1)$$

$$\delta O_2/N_2 = \delta O_2/N_{2raw} - 4 \cdot \delta^{15}N \quad (2)$$

The final precision (pooled SD) for our new set of data is 0.02 ‰ for $\delta^{18}O_{atm}$ and 0.79 ‰ for $\delta O_2/N_2$.

3 Results and discussion

Figure 1 shows the full EDC $\delta^{18}O_{atm}$ dataset, which has a mean temporal resolution of 1.1 ka thanks to our new dataset completing the records of Dreyfus et al. (2007,

CPD
11, 1437–1477, 2015

2008); Bazin et al. (2013) between 300–800 ka, and Landais et al. (2013) over MIS 5. The data depict variations that coincide with those of precession, together with larger changes associated with glacial terminations. There is an excellent overall agreement between variations in precession and the lagged precession signal in $\delta^{18}O_{atm}$, with two exceptions corresponding to periods of low eccentricity: between 350 and 450 ka (MIS12-11-10) and around 700 to 800 ka. As already observed by Dreyfus et al. (2007), our new results illustrate that precession-driven variations in $\delta^{18}O_{atm}$ are reduced during these periods of low eccentricity. Moreover, with the addition of our new data, the tuning performed by Dreyfus et al. (2007) between 530–550 ka is not as straightforward as previously presented. Still, this stays within the uncertainties associated with $\delta^{18}O_{atm}$ orbital tuning and has no impact on the chronology construction.

Spectral analyses of the $\delta^{18}O_{atm}$ record spanning 300–800 ka (Fig. 2) confirm earlier results obtained by Dreyfus et al. (2007) for EDC, and those obtained for Vostok and Dome F data over the last 400 ka (Petit et al., 1999; Kawamura et al., 2007). The major peaks are observed for periods of 100, 19–23, and 41 ka (by decreasing amplitude) and correspond respectively to the eccentricity and/or glacial–interglacial climatic variations, precession and obliquity bands.

Our new data allow us to establish a record of $\delta O_2/N_2$ from 380 to 800 ka measured on well-conserved ice (Fig. 1). Series A (392–473 ka) and B (706–800 ka) were measured in 2007–2008 (Landais et al., 2012) and are complemented by our new set of data (Series C). The mean temporal resolution of the complete $\delta O_2/N_2$ record is 2.35 ka, with two main gaps (220 between 160–380 ka and 20 between 470–490 ka). The pooled SDs of each dataset vary between 0.3 and 1 ‰ (A: 0.32 ‰, B: 1.03 ‰; C: 0.79 ‰).

When compared with earlier data affected by gas loss (Landais et al., 2012), our data show the same timing of variations of $\delta O_2/N_2$ that coincide with those of local summer solstice insolation at Dome C (Appendix A). However, the relative strengths of minima and maxima of $\delta O_2/N_2$ do not scale with those of summer insolation. Large amplitudes of summer insolation cycles are associated with relatively small amplitudes

CPD
11, 1437–1477, 2015

of the corresponding cycles in $\delta O_2/N_2$ and vice versa (Fig. 1) and only 13 % of the variance of the raw $\delta O_2/N_2$ data is explained by summer solstice insolation. Finally, the new record reveals an overall decreasing trend of $\delta O_2/N_2$ over the last 800 ka at EDC (0.78 ± 0.08 ‰/100 ka), confirming the observations of Landais et al. (2012) on their composite curve (Appendix A). Moreover, this feature was already identified during the last 400 ka at Vostok (0.56 ± 0.33 ‰/100 ka) and 360 ka at Dome F (0.56 ± 0.28 ‰/100 ka). We conclude that the long term decreasing trend of $\delta O_2/N_2$ with time is not an artifact due to the gas loss correction, but it may still be linked with a different preservation of the air with varying depth in the ice core. Long term changes in the enclosing process or modification in the atmospheric ratio O_2/N_2 can also be evoked.

The spectral analysis of the new EDC $\delta O_2/N_2$ record between 380–800 ka (Fig. 2) depicts peaks associated with the precession and obliquity bands (19–23 and 41 ka), together with a 100 ka periodicity. This 100 ka period was neither observed in $\delta O_2/N_2$ records from other Antarctic ice cores (Bender, 2002; Kawamura et al., 2007) nor in the composite EDC record of Landais et al. (2012).

The 100 ka peak is also absent from the power spectrum of summer solstice insolation, independently of the time window considered (Fig. 2). The 100 ka signal in $\delta O_2/N_2$, most strongly imprinted between 500 and 700 ka, arises from pronounced minima in the $\delta O_2/N_2$ record at 450, 550 and 650 ka. These minima occur during glacial periods characterized by low eccentricity, and therefore coincide with local insolation minima (arrows on Fig. 1). The 100 ka periodicity identified in the EDC $\delta O_2/N_2$ record between 380–800 ka, and absent from records spanning 0–400 ka may thus arise from a reduced influence of precession-driven insolation changes on snow metamorphism during eccentricity minima, similarly to the parallel reduced precession-driven signal in $\delta^{18}O_{atm}$. Such a reduced influence would leave room for other factors to impact EDC $\delta O_2/N_2$, such as local climatic parameters. Indeed, records of local climate (e.g. water stable isotopes and inferred changes in local temperature and accumulation rate, dust) exhibit a strong peak at 100 ka, characteristic of glacial–interglacial cycles (Masson-Delmotte et al., 2010; Lambert et al., 2008). The 100 ka periodicity in

CPD
11, 1437–1477, 2015

EDC $\delta O_2/N_2$ could therefore arise from an influence of local climate related parameters, which would be more strongly expressed under a low eccentricity context.

3.1 MIS 5 Antarctic inter-comparison

Our EDC $\delta O_2/N_2$ record displays variability in the precession and obliquity ranges, as well as minima and maxima that highlight clear similarities with local summer insolation. However, neither the modulation in amplitude nor the 100 ka signal are related to local summer insolation, pointing to other local influences such as changes in surface energy budget, firn dust content, changes in temperature and accumulation rate, which could affect snow metamorphism and firnification processes. While variations in summer solstice insolation are expected to be very similar in all East Antarctic ice core sites, differences in site characteristics (e.g. snow properties, meteorological situation, mean climate) may cause differences in the $\delta O_2/N_2$ signals from different ice cores, if local processes have a significant influence. This motivates a comparison of $\delta O_2/N_2$ signals from three ice cores drilled in the East Antarctic plateau: Dome F, Vostok and EDC. Present-day conditions at these three dry and particularly cold sites depict differences in the distance to open ocean, elevation (within 577 m), albedo (within 3 %), wind speed (a factor of two), accumulation (within 15 %) and mean annual temperature (within 2.5 °C) (Table 1).

Thanks to our new $\delta O_2/N_2$ data, we now have records of both $\delta O_2/N_2$, $\delta^{18}O_{atm}$ and water isotopes over MIS 5 from EDC, Dome F and Vostok. This MIS 5 period is also of particular interest since it is characterized by large precession parameter variations, together with large glacial-interglacial changes in Antarctic temperature, with warmer-than-present reconstructed interglacial temperatures (Sime et al., 2009; Stenni et al., 2010; Masson-Delmotte et al., 2011; Uemura et al., 2012).

Figure 3 displays the $\delta O_2/N_2$ records from Dome F (on the DFO-2006 time scale), EDC and Vostok (both on their respective AICC2012 chronologies) from 150 to 100 ka. We observe the same orbital scale variations from all three records, i.e. a $\delta O_2/N_2$

CPD
11, 1437–1477, 2015

maximum at around 126 ka bracketed by 2 minima at 115 and 135 ka. Two major differences are still noticeable:

- A lower $\delta O_2/N_2$ mean value and greater amplitude in variations at Vostok than at Dome F and EDC.
- A site-specific high frequency variability. For instance, between 100–115 ka, EDC and Vostok $\delta O_2/N_2$ records show a double peak that is not observed at Dome F and significantly larger than measurements uncertainties.

The gas loss corrections applied on the Dome F and Vostok $\delta O_2/N_2$ records may explain part of these discrepancies. The resolution of the records (2.3 ka for EDC, 1.5 ka for Vostok and 1.2 ka for Dome F between 100–150 ka) limits the comparison of high frequency variations observed between 100 and 115 and around 126 ka. In the Greenland GISP2 ice core, it has been shown that $\delta O_2/N_2$ can display millennial scale variability, in relationship with glacial climatic variability (Suwa and Bender, 2008a). Only high-resolution measurements conducted on well-conserved ice could allow us to have an objective discussion of high frequency signals in Antarctic ice.

All three $\delta O_2/N_2$ records present variations that occur simultaneously with the ones of the local summer solstice insolation target curves (Fig. 3). This is expected since the different ice core chronologies used in Fig. 3 are based at least partially on the alignment of the $\delta O_2/N_2$ signal on the summer solstice insolation curve. An intriguing feature arises from the comparison of the lags between $\delta O_2/N_2$, $\delta^{18}O_{atm}$ and $\delta^{18}O_{ice}$ within each ice core (Fig. 3). While the $\delta O_2/N_2$ records of the three sites seem aligned, Dome F $\delta^{18}O_{atm}$ and $\delta^{18}O_{ice}$ exhibit a fingerprint of Termination II occurring 2 ka earlier than the ones recorded in Vostok and EDC (as observed on water stable isotope optima, Fig. 3 and Bazin et al., 2013). The same shift between Dome F and EDC/Vostok $\delta^{18}O_{atm}$ and $\delta^{18}O_{ice}$ records is also observed for the glacial inception. This shift of several thousands years between chronologies highlights the limitation of orbital tuning in ice cores, even if the chronologies are also constrained by glaciological modeling (Kawamura et al., 2007; Bazin et al., 2013). It also strengthens the fact that quite large

CPD
11, 1437–1477, 2015

uncertainties should be associated with $\delta O_2/N_2$ orbital tuning. An objective alignment between $\delta O_2/N_2$ and orbital target is difficult to obtain because of low resolution and scattering of $\delta O_2/N_2$ data.

Still, the $\delta O_2/N_2$ minimum at the timing of Termination II (arrows on Fig. 3) is clearly later at EDC than at Dome F. If only local summer solstice insolation was a direct driver of $\delta O_2/N_2$ changes, one would expect the three $\delta O_2/N_2$ records to be exactly synchronous. We thus look for alternative explanations for a modulation of the lag between summer solstice insolation and $\delta O_2/N_2$.

First, differences between sites may result from a different response of snow metamorphism and therefore $\delta O_2/N_2$ to orbital forcing. One important assumption for the process linking $\delta O_2/N_2$ and orbital forcing is that snow metamorphism is maximum at peak temperature (Kawamura et al., 2007) so that summer solstice insolation curve should be taken as orbital target for $\delta O_2/N_2$ variations. At Dome F, the current seasonal cycle of surface snow temperature measurements shows maximum values at the summer solstice (21 December, Kawamura et al., 2007). At Vostok, the maximum of surface snow temperature is observed about 10 days later, close to 30 December (continuous measurements since 2010, Lefebvre et al., 2012; J.-R. Petit, personal communication, 2013). At Dome C, 3 years continuous measurements of surface snow temperature between 2006–2009 have shown that the maximum of temperature occurs 15–20 days after the summer solstice (Landais et al., 2012, confirmed by the continuous measurements since then). These regional differences highlight the fact that, today, surface snow temperature does not reach its summer maximum in phase with local summer solstice insolation. As a consequence, different insolation target curves for $\delta O_2/N_2$ should be considered for the different sites if the observations performed for present day conditions are also valid for the past. Following this observation, we have tried to use 30 December and 15 January insolation curves as respective orbital targets for EDC and Vostok $\delta O_2/N_2$ records. However, using such orbital targets strengthens the lag between the Dome F and Vostok-EDC age scales over MIS 5.

CPD
11, 1437–1477, 2015

Second, we explore if inter-site differences in surface albedo could explain differences in the energy input for surface snow metamorphism (Picard et al., 2012). Surface albedo is currently measured over East Antarctica with MODIS multispectral imager on board TERRA and AQUA satellites. Data collected since 2001 enable to compare the albedo of our three sites of interest (Table 1). For this purpose, White Sky broadband albedo data (surface albedo under perfectly diffuse illumination conditions) were extracted from MCD43A3 products (http://www.umb.edu/spectralmass/terra_aqua_modis/v006). Only values for which local solar noon sun zenith angle is less than 65° and high quality flags (QA = 0 in MCD43A2 products) are considered (Schaaf et al., 2011). They show similar values at Vostok and EDC (0.83), and significantly lower values at Dome F (0.80). This implies that, today, about 15 % more incoming solar radiations are absorbed by Dome F surface snow and can act on its metamorphism. However, surface metamorphism is not simply related to surface albedo. This can be investigated using the grain index time series developed by Picard et al. (2012). The amplitude of diurnal cycles and grain size near the surface indicate more metamorphism at Dome C than at Dome F. We note that the largest amplitude of grain growth is observed at South Pole, despite a high local albedo and no diurnal cycle. While present day data provide a hint for possible differences in surface snow metamorphism, further studies are needed to better understand how the surface energy budget controls the surface and subsurface snow metamorphism, and how it can explain the differences in $\delta O_2/N_2$ mean level and phasing between $\delta O_2/N_2$ and insolation forcing at different sites.

Third, we investigate how changes in layering or snow microstructure during the firnification processes can affect $\delta O_2/N_2$. Several indices indeed suggest that $\delta O_2/N_2$ is not only influenced by the energy received at the surface of snow but also by firnification processes, which themselves depend on climatic conditions such as accumulation rate, firn temperature, impurity content of the snow (Hutterli et al., 2010). We have thus searched for local climatic influence on $\delta O_2/N_2$ focusing first on accumulation rates. No significant correlation can be identified between EDC accumulation

CPD
11, 1437–1477, 2015

rate produced by AICC2012 and $\delta O_2/N_2$ variations (R = 0.107 between 380–800 ka). Moreover, no direct link can be established between the relative values of accumulation rates and $\delta O_2/N_2$ values comparing Dome F, Vostok and EDC over the MIS 5 period (Appendix B). Still, this investigation is limited by the fact that the Vostok and Dome F $\delta O_2/N_2$ records are corrected for gas loss. It is also possible to face different compensating effects of accumulation rate and local temperature that could be site-specific (Bender, 2002; Hutterli et al., 2010).

Finally, changes in dust concentration have been suggested to potentially influence firn density and hence air trapping (Hörhold et al., 2012; Freitag et al., 2013). Records of dust concentration spanning MIS 5 are available for EDC (Lambert et al., 2008) and Vostok (Petit et al., 1999). There is no significant difference between the dust concentration of Vostok and EDC regarding their amplitude and timing of changes, so they should have the same effect at both sites. The lack of published $\delta O_2/N_2$ and dust records from Dome F precludes investigations of the differences between Dome F and Vostok-EDC. Moreover, subsurface processes and reworking of surface snow by the wind are known to have an influence on actual firnification, as a result this should have an impact on the $\delta O_2/N_2$ trapping process (Fujita et al., 2012), even under glacial climatic conditions.

This study provides support for more complex processes affecting the $\delta O_2/N_2$ than just the local summer solstice modulation. We cannot yet explain the origin of such site differences of the $\delta O_2/N_2$ records as we are limited by the lack of available data ($\delta O_2/N_2$ on well-conserved ice for Vostok and Dome F, dust records for Dome F, CH_4 for Dome F) and by our current understanding of firnification processes. However, from the available information we can point to a cautious use of orbital age markers inferred from $\delta O_2/N_2$ with possible differences from one site to another. Based on the inter-site differences, we recommend to use an uncertainty of 3–4 ka, and to combine these data with other dating tools.

CPD
11, 1437–1477, 2015

3.2 $\delta O_2/N_2$–$\delta^{18}O_{atm}$ lag

A lag of $\delta^{18}O_{atm}$ vs. precession was observed over the last termination at Vostok, EDC and GISP2 with values of 5.8, 5.9 and 5.3 ka on the FGT1, EDC3 and Meese/Sowers chronologies respectively (Dreyfus et al., 2007; Petit et al., 1999; Parrenin et al., 2004, 2007; Bender et al., 1994; Meese et al., 1994). On the new AICC2012 chronology, the lag of $\delta^{18}O_{atm}$ with precession over Termination I is now of 5.6 ka for Vostok and 5.5 ka for EDC.

During Termination II, recently published high-resolution $\delta^{18}O_{atm}$ measurements (Landais et al., 2013) together with the AICC2012 chronology (Bazin et al., 2013) also give a $\sim$ 5 ka phase lag (5.2 ka) between precession and $\delta^{18}O_{atm}$. Bazin et al. (2013) have shown an excelent agreement for the timing of Termination II on a purely orbital ice core chronology (AICC2012 using only ice core orbital age markers over Termination II) and an independent speleothem chronology based on U/Th Dating (Cheng et al., 2009). This comparison rely on the assumption that abrupt variations in CH_4 and calcite $\delta^{18}O$ are synchronous. While this assumption was explicitly used to build the EDC3 chronology (Parrenin et al., 2007; Waelbroeck et al., 2008), this is not the case for AICC2012, which provides high confidence in the accuracy of this chronology for Termination II.

The determination of the lag between $\delta^{18}O_{atm}$ and precession for earlier terminations is more complicated. Indeed, it requires an absolute chronology that is independent from orbital tuning based on $\delta^{18}O_{atm}$. Similarly, determining the phase lag between $\delta O_2/N_2$ and summer solstice insolation is not possible in the absence of an alternative timescale free from $\delta O_2/N_2$ constraints. However, we can still progress on the issue of relative phase lags between $\delta^{18}O_{atm}$, $\delta O_2/N_2$ and orbital targets by studying the relationships between $\delta O_2/N_2$ and $\delta^{18}O_{atm}$. Indeed, even if the orbital targets of both parameters are close and without significant lags between them (less than 500 years over the last 800 ka, Fig. 4), $\delta^{18}O_{atm}$ and $\delta O_2/N_2$ variations are due to very different mechanisms (remote for $\delta^{18}O_{atm}$, local for $\delta O_2/N_2$). As a consequence, it is very un-

CPD
11, 1437–1477, 2015

likely that variations of $\delta^{18}O_{atm}$ and $\delta O_2/N_2$ lags relative to their orbital targets would occur simultaneously and compensate each other. These changes should then be visible on the lag between $\delta O_2/N_2$ and $\delta^{18}O_{atm}$.

Based on the good agreement of the Vostok and EDC $\delta O_2/N_2$ records over MIS 5, we have combined the full Vostok (0–400 ka) and EDC (380–800 ka) $\delta O_2/N_2$ and $\delta^{18}O_{atm}$ records (Fig. 4). We have re-interpolated the $\delta O_2/N_2$ and the reverse of $\delta^{18}O_{atm}$, in order to account for their negative correlation, every 1 ka. There is a close resemblance of the interpolated and original data. In order to calculate the phase delay, we have then normalized these two interpolated records and filtered them between 15 and 100 ka, using wavelet transform.

During periods of weak eccentricity (e.g. around 400 and before 720 ka), there is no clear correspondence between the variations of $\delta O_2/N_2$ and $\delta^{18}O_{atm}$ on one hand and the variations of their orbital target curves on the other hand, as previously noted (Dreyfus et al., 2007; Landais et al., 2012). During these periods, the variations of insolation in the precession band are probably too small to be imprinted in either $\delta O_2/N_2$ or $\delta^{18}O_{atm}$ records. Moreover, the new $\delta O_2/N_2$ record present missing data between 470–490 ka, so that the phase delay cannot be calculated over this period. Finally, the most recent 100 ka correspond to a period of low eccentricity and the $\delta O_2/N_2$ signal does not display any variability comparable to that of the insolation curve (before the air bubbles/clathrates transition). As a consequence, we disregard these periods for our discussion of the phase delay (not shown on Fig. 4). This also means that the orbital tuning through $\delta^{18}O_{atm}$ and $\delta O_2/N_2$ is much less reliable over these periods. We therefore recommend excluding such orbital tie points during large eccentricity minima, or considering them with larger uncertainties. On Fig. 4, we can see that the $\delta O_2/N_2$ records (original and filtered) do not present the same variability as the local summer solstice insolation during MIS 13. As a result, it is not possible to discuss the phase delay between $\delta O_2/N_2$ and $\delta^{18}O_{atm}$ over this period. The time intervals covered over the following discussion correspond to 100–350 and 530–720 ka.

CPD
11, 1437–1477, 2015

During the remaining intervals of intermediate to strong eccentricity, the phase delay between $\delta O_2/N_2$ and $\delta^{18}O_{atm}$ varies between −6 and −1 ka. These phase delay values are significant as the re-interpolated and filtered curves present the same variability as the original data (Fig. 4). For Termination II, we obtain a $\delta^{18}O_{atm}$ vs. $\delta O_2/N_2$ phase delay of 4.5 ka, which is in good agreement with the $\delta^{18}O_{atm}$ vs. precession lag observed on raw data and a zero phase between $\delta O_2/N_2$ and summer solstice insolation as displayed on Fig. 3. On Fig. 4, we observe that the phase delay between $\delta O_2/N_2$ and $\delta^{18}O_{atm}$ is minimal during MIS 6–7, the end of MIS 9, MIS 15 and MIS 17, with the minimum value occurring during MIS 15 (−1.1 ka). These periods are marked by high eccentricity levels together with intermediate ice-sheet extents (i.e. neither full glacial conditions nor extremely warm interglacial conditions). On the contrary, local maxima of the $\delta O_2/N_2$–$\delta^{18}O_{atm}$ phase delay are observed for MIS 8 (−5 ka) and MIS 16 (−3 ka).

Part of the variations in the phase delay between $\delta O_2/N_2$ and $\delta^{18}O_{atm}$ may be due to the uncertainty in the age difference between ice and gas ages since $\delta^{18}O_{atm}$ is expressed on a gas timescale while $\delta O_2/N_2$ is on an ice timescale. Such uncertainty is largest during glacial periods, due to the impact of glacial climate conditions on firn processes. This uncertainty always stays below 1 ka, and therefore cannot explain the observed variations in phase delay between $\delta O_2/N_2$ and $\delta^{18}O_{atm}$. We argue that the large variations of the phase delay observed between $\delta O_2/N_2$ and $\delta^{18}O_{atm}$ are mainly due to variations in the phase delay between $\delta^{18}O_{atm}$ and precession, as $\delta O_2/N_2$ is synchronous with local insolation and there is nearly no differences in timing of insolation and precession variations. Indeed, the link between precession and $\delta^{18}O_{atm}$ is not direct and involves global modifications of the low latitude water cycle and biosphere productivity. On the opposite, while the exact mechanism linking $\delta O_2/N_2$ to summer solstice insolation is not yet fully understood, there is no doubt that it involves local firn processes with a faster response time.

Many reasons are invoked to explain the phase lag between precession and $\delta^{18}O_{atm}$. As evidenced over Terminations I and II and over the last 240 ka, $\delta^{18}O_{atm}$ variations are closely related to the dynamic of the low latitude hydrological cycle (Wang et al.,

CPD
11, 1437–1477, 2015

2008; Severinghaus et al., 2009; Landais et al., 2007, 2010, 2013; Cheng et al., 2009). Monsoons are influenced by orbital forcing, with a strong imprint of precession (Wang et al., 2008; Braconnot et al., 2008), but also by millennial scale variability (Wang et al., 2001; Marzin et al., 2013). The Heinrich event 1 is for instance associated with a weak monsoon interval (e.g. Denton et al., 2010). We note that Termination I and Termination II are associated with large Heinrich events during the first part of the deglaciation, when orbital forcing already acts on sea level and global climate, including Antarctic temperature (Landais et al., 2013).

In order to study the possible link between variations of the $\delta O_2/N_2$–$\delta^{18}O_{atm}$ phase delay and the occurrence of Heinrich events, we confront our results to an Ice Rafted Debris (IRD) proxy (Ca/Sr) from the marine cores U1302/03 and U1308 located within the IRD belt of North Atlantic (Hodell et al., 2008; Channell et al., 2012; Channell and Hodell, 2013). As the two sites are located on the western and eastern borders of the IRD belt respectively, spikes present within both Ca/Sr records indicate the occurrence of Heinrich-like events over the last 800 ka. The Ca/Sr can be considered as an IRD proxy as its spikes correspond to rich detrial carbonate layers, characterizing IRD from the Laurentide ice sheet. At the bottom of Figure 4 are represented the oxygen isotopes and Ca/Sr records of marine cores U1302/03 and U1308 on their respective chronologies. We can see that Ca/Sr spikes recorded in both marine cores occur at the same periods as the local maximum of the $\delta O_2/N_2$–$\delta^{18}O_{atm}$ phase delay (within chronologies uncertainties, red arrows on Fig. 4). On the contrary, periods associated with the smallest lags between $\delta O_2/N_2$ and $\delta^{18}O_{atm}$ present Ca/Sr spikes in the U1302/03 marine core, but not in the U1308. Channell et al. (2012) speculate that these events correspond to debris flows or glacial-lake drainage events caused by changes in hydrological budget or changes in base level. Consequently, the marine data can be interpreted as evidence for the occurrence of Heinrich-like events during MIS 8 and MIS 16. We suggest that, during these two periods, the Heinrich-like events delay the response of monsoons and thus $\delta^{18}O_{atm}$ with respect to precessional forcing. By contrast, where we detect the smallest lags between precession and $\delta^{18}O_{atm}$

CPD
11, 1437–1477, 2015

(Fig. 4), no Heinrich-like events are observed within both marine cores. We therefore explain the minimum lag between $\delta^{18}O_{atm}$ and precession during MIS 6–7, the end of MIS 9, MIS 15 and MIS 17 by the combination of three factors: minimum effects of ice volume changes (due to intermediate ice sheet extent), strong impact of precession on monsoons (due to high eccentricity), and the absence of Heinrich-like event.

In summary, our datasets suggest that the phase lag between $\delta^{18}O_{atm}$ and precession can vary between 1 to more than 6 ka, with minimum values during periods of strong eccentricity and intermediate ice volume (no Heinrich events). This varying lag results from the complex interplay of orbital and millennial variations affecting changes in sea-water isotopic composition, tropical water cycle, and biosphere productivity. The phase identified over Termination I and II may not apply for earlier transitions without Heinrich events. It implies that the phase lag of Termination I may provide an upper estimation for the associated uncertainty range.

4 Conclusions and perspectives

We have presented new measurements of $\delta O_2/N_2$ and $\delta^{18}O_{atm}$ performed on well-conserved ice from EDC over MIS 5 and between 380–800 ka. As a result, we now have a new reference $\delta O_2/N_2$ curve between 380–800 ka with a mean resolution of 2.35 ka, confirming earlier observations about a decreasing trend over the last 800 ka and timing of orbital scale variations. The spectral analysis of the new $\delta O_2/N_2$ curve between 380–800 ka showed for the first time a significant peak in the periodicity band characterising eccentricity and glacial–interglacial variations, hence suggesting that processes other than local summer insolation do impact $\delta O_2/N_2$ on glacial–interglacial scales. This should motivates further studies to unveil the processes at play both for long term trends and at glacial–interglacial/eccentricity timescales.

Thanks to our comprehensive datasets, we have been able for the first time to compare the sequence of events between water isotopes, $\delta O_2/N_2$ and $\delta^{18}O_{atm}$ for three Antarctic ice cores (EDC, Vostok and Dome F), over MIS 5. Significant differences have

CPD
11, 1437–1477, 2015

been observed, which cannot be entirely explained by differences in resolution or by the corrections applied on $\delta O_2/N_2$ records of Dome F and Vostok. In particular, we have evidenced that the alignment of $\delta O_2/N_2$ on the summer solstice insolation signal may vary by ~ 2 ka from site to site. This may be due to an influence of local climatic parameters on the $\delta O_2/N_2$. This demonstrates the interest of the multi-proxy, multi-ice cores chronology approach, which is therefore crucial to correctly assess the uncertainties associated with individual age markers. Again the mechanisms responsible for local $\delta O_2/N_2$ variations remain to be understood. This is particularly important over periods of low eccentricity when the insolation variations are not well imprinted in the $\delta O_2/N_2$ records (350–450 and 700–800 ka). The $\delta O_2/N_2$ orbital tuning method should not be used alone during these periods.

Moreover, we have calculated the delay between $\delta O_2/N_2$ and $\delta^{18}O_{atm}$ over the last 800 ka by coupling Vostok and EDC data. This lag has varied from 1 to 6 ka with minimum values during MIS 6–7, the end of MIS 9, MIS 15 and MIS 17, corresponding to periods of high eccentricity and intermediate ice-sheet extent. Based on results observed over MIS 5, we make the assumption that $\delta O_2/N_2$ is synchronous with summer solstice insolation and that this lag is mainly due to variations in the relationship between $\delta^{18}O_{atm}$ and precession. It has been shown over Terminations I and II that the $\delta^{18}O_{atm}$ response to precession can be delayed during Heinrich events, associated with weak monsoon intervals. The small values of the phase delay observed during MIS 6–7, the end of MIS 9, MIS 15 and MIS 17 are therefore attributed to a lack of Heinrich-like event during these periods, combined with high eccentricity and intermediate ice sheet extent.

In order to refine this analysis, new measurements on well-conserved ice of $\delta O_2/N_2$ and $\delta^{18}O_{atm}$ are needed between 160–380 and 470–490 ka for the EDC ice core, and over the last 400 ka for Vostok and Dome F ice cores. Integrating Dome F on the AICC2012 age scale will be crucial to improve the Antarctic chronology. This methodology will then permit to investigate properly the causes of inter-site differences during MIS 5, and assess if similar features arise during other time periods. New measure-

CPD
11, 1437–1477, 2015

ments on well-conserved ice together with constraints on past changes in dust concentration and accumulation rates should allow us to assess whether there is any robust link between variables that can potentially affect metamorphism such as dust content and accumulation rate. Moreover, further studies are needed on processes affecting surface snow in order to better understand its metamorphism. Finally, it is crucial to better understand how the low latitude water cycle and biosphere productivity influence the $\delta^{18}O_{atm}$ and its lag with precession in order to estimate correctly the uncertainty associated with the $\delta^{18}O_{atm}$ orbital tuning methods. To do so, it is necessary to improve uncertainties associated with ice and marine cores. The development of multi-archives dating tool should permit to synchronize records from different archives and thus discuss in more details how the Heinrich events influence the $\delta^{18}O_{atm}$ lag with precession.

Appendix A: EDC $\delta O_2/N_2$ records

We have compared the $\delta O_2/N_2$ composite curve of Landais et al. (2012), corrected for gas loss, with our new record only measured on well-conserved ice (Fig. A1). We observe nearly the same timing of variations. We conclude that the increased resolution and accuracy of our new dataset do not affect the position of mid-slope variations and therefore orbital tuning. The uncertainty associated with the mid-slope identification is always smaller than the uncertainty associated with $\delta O_2/N_2$ orbital tuning. Note that we have identified an error in the earlier composite curve due to the use of gas age instead of ice age for the time period 400 to 450 ka. This error has been corrected and explains the difference between our new record and the one of Landais et al. (2012). Compared to the Landais et al. (2012) composite curve, the new record presents smaller amplitudes of variations, possibly because of gas loss corrections. Our new data record a long term decrease of $\delta O_2/N_2$ over time of 0.78 ± 0.08 ‰/100 ka, which is very close to the long term decrease of 0.86 ± 0.14 ‰/100 ka, deduced from the Landais et al. (2012) composite curve.

CPD
11, 1437–1477, 2015

Appendix B: Appendix B: $\delta O_2/N_2$ and accumulation

For East Antarctic ice cores, accumulation rates are usually deduced from water stable isotopes and then adjusted by chronological constraints and ice flow modeling. Here, we use the accumulation rates produced in the AICC2012 chronology. For Dome F, we have transferred the accumulation rate deduced from ice flow modeling (Parrenin et al., 2007, DFGT-2006) on the DFO-2006 chronology. In order to investigate a possible link between $\delta O_2/N_2$ and accumulation rate, we have interpolated them with a 1 ka step between 100–150 ka, and compared their values for EDC, Vostok and Dome F.

Four different time intervals are identified from changes in accumulation rates (Fig. B1):

1. Low accumulation rates during the penultimate glacial period, prior to 140 ka.
2. Accumulation increase during the glacial–interglacial transition.
3. High accumulation rates during the interglacial period and decreasing rates during glacial inception.
4. Last glacial period since 100 ka.

Note that the timing of these 4 phases can differ amongst the three ice core records. Figure B1 shows that no link can be established between accumulation rate and $\delta O_2/N_2$ values. This study is of course limited by the fact that Vostok and Dome F $\delta O_2/N_2$ data are corrected for gas loss, and by the lack of accumulation rate data directly inferred from the DFO-2006 age scale. While no first-order conclusion can be reached, this study should be repeated as soon as data measured on well-conserved ice will be available for Dome F and Vostok over this period.

Acknowledgements. We thank Jean-Robert Petit and Laurent Arnaud for the help with the surface temperature data of Vostok and EDC. We thank James Channel for the marine cores data. The present research project No 902 has been performed at Concordia Station and was supported by the French Polar Institute (IPEV). This project was funded by the "Fondation

CPD
11, 1437–1477, 2015

de France Ars Cuttoli" and the "ANR Citronnier". The research leading to these results has received funding from the European Union's Seventh Framework programme (FP7/2007-2013) under grant agreement no 243908, "Past4Future. Climate change – Learning from the past climate". This is Past4Future contribution number XX. This is LSCE contribution no XX.

References

Battle, M., Bender, M., Sowers, T., Tans, P. P., Butler, J. H., Elkins, J. W., Ellis, J. T., Conway, T., Zhang, N., Lang, P., and Clarket, A. D.: Atmospheric gas concentrations over the past century measured in air from firn at the South Pole, Nature, 383, 231–235, doi:10.1038/383231a0, 1996. 1441

Bazin, L., Landais, A., Lemieux-Dudon, B., Toyé Mahamadou Kele, H., Veres, D., Parrenin, F., Martinerie, P., Ritz, C., Capron, E., Lipenkov, V., Loutre, M.-F., Raynaud, D., Vinther, B., Svensson, A., Rasmussen, S. O., Severi, M., Blunier, T., Leuenberger, M., Fischer, H., Masson-Delmotte, V., Chappellaz, J., and Wolff, E.: An optimized multi-proxy, multi-site Antarctic ice and gas orbital chronology (AICC2012): 120–800 ka, Clim. Past, 9, 1715–1731, doi:10.5194/cp-9-1715-2013, 2013. 1439, 1442, 1443, 1445, 1448, 1452, 1469, 1472

Bender, M.: Orbital tuning chronology for the Vostok climate record supported by trapped gas composition, Earth Planet. Sc. Lett., 204, 275–289, doi:10.1016/S0012-821X(02)00980-9, 2002. 1441, 1442, 1446, 1451

Bender, M., Sowers, T., and Labeyrie, L.: The Dole effect and its variations during the last 130 000 years as measured in the Vostok ice core, Global Biogeochem. Cy., 8, 363–376, doi:10.1029/94GB00724, 1994. 1440, 1452

Bender, M., Sowers, T., and Lipenkov, V.: On the concentrations of O_2, N_2, and Ar in trapped gases from ice cores, J. Geophys. Res.-Atmos., 100, 18651–18660, doi:10.1029/94JD02212, 1995. 1442

Braconnot, P., Marzin, C., Grégoire, L., Mosquet, E., and Marti, O.: Monsoon response to changes in Earth's orbital parameters: comparisons between simulations of the Eemian and of the Holocene, Clim. Past, 4, 281–294, doi:10.5194/cp-4-281-2008, 2008. 1455

Buiron, D., Chappellaz, J., Stenni, B., Frezzotti, M., Baumgartner, M., Capron, E., Landais, A., Lemieux-Dudon, B., Masson-Delmotte, V., Montagnat, M., Parrenin, F., and Schilt, A.:

CPD
11, 1437–1477, 2015

TALDICE-1 age scale of the Talos Dome deep ice core, East Antarctica, Clim. Past, 7, 1–16, doi:10.5194/cp-7-1-2011, 2011. 1439

Caley, T., Malaizé, B., Revel, M., Ducassou, E., Wainer, K., Ibrahim, M., Shoeaib, D., Migeon, S., and Marieu, V.: Orbital timing of the Indian, East Asian and African boreal monsoons and the concept of a "global monsoon", Quaternary Sci. Rev., 30, 3705–3715, doi:10.1016/j.quascirev.2011.09.015, 2011. 1440

Channell, J., Hodell, D., Romero, O., Hillaire-Marcel, C., de Vernal, A., Stoner, J., Mazaud, A., and Röhl, U.: A 750-kyr detrital-layer stratigraphy for the North Atlantic (IODP Sites U1302–U1303, Orphan Knoll, Labrador Sea), Earth Planet. Sc. Lett., 317–318, 218–230, doi:10.1016/j.epsl.2011.11.029, 2012. 1455

Channell, J. E. T. and Hodell, D. A.: Magnetic signatures of Heinrich-like detrital layers in the Quaternary of the North Atlantic, Earth Planet. Sc. Lett., 369, 260–270, doi:10.1016/j.epsl.2013.03.034, 2013. 1455

Cheng, H., Edwards, R. L., Broecker, W. S., Denton, G. H., Kong, X., Wang, Y., Zhang, R., and Wang, X.: Ice age terminations, Science, 326, 248–252, doi:10.1126/science.1177840, 2009. 1452, 1455

Denton, G. H., Anderson, R. F., Toggweiler, J. R., Edwards, R. L., Schaefer, J. M., and Putnam, A. E.: The last glacial termination, Science, 328, 1652–1656, doi:10.1126/science.1184119, 2010. 1455

Dreyfus, G. B., Parrenin, F., Lemieux-Dudon, B., Durand, G., Masson-Delmotte, V., Jouzel, J., Barnola, J.-M., Panno, L., Spahni, R., Tisserand, A., Siegenthaler, U., and Leuenberger, M.: Anomalous flow below 2700 m in the EPICA Dome C ice core detected using δ^{18}O of atmospheric oxygen measurements, Clim. Past, 3, 341–353, doi:10.5194/cp-3-341-2007, 2007. 1440, 1443, 1444, 1445, 1452, 1453, 1469

Dreyfus, G. B., Raisbeck, G. M., Parrenin, F., Jouzel, J., Guyodo, Y., Nomade, S., and Mazaud, A.: An ice core perspective on the age of the Matuyama-Brunhes boundary, Earth Planet. Sc. Lett., 274, 151–156, doi:10.1016/j.epsl.2008.07.008, 2008. 1443, 1445, 1469

Freitag, J., Kipfstuhl, S., Laepple, T., and Wilhelms, F.: Impurity-controlled densification: a new model for stratified polar firn, J. Glaciol., 59, 1163–1169, doi:10.3189/2013JoG13J042, 2013. 1442, 1451

Fujita, S., Enomoto, H., Fukui, K., Iizuka, Y., Motoyama, H., Nakazawa, F., Sugiyama, S., and Surdyk, S.: Formation and metamorphism of stratified firn at sites located under spatial vari-

CPD
11, 1437–1477, 2015

ations of accumulation rate and wind speed on the East Antarctic ice divide near Dome Fuji, The Cryosphere Discuss., 6, 1205–1267, doi:10.5194/tcd-6-1205-2012, 2012. 1451
Hodell, D. A., Channell, J. E. T., Curtis, J. H., Romero, O. E., and Röhl, U.: Onset of "Hudson Strait" Heinrich events in the eastern North Atlantic at the end of the middle Pleistocene transition (~640 ka)?, Paleoceanography, 23, 4218, doi:10.1029/2008PA001591, 2008. 1455
Hörhold, M., Laepple, T., Freitag, J., Bigler, M., Fischer, H., and Kipfstuhl, S.: On the impact of impurities on the densification of polar firn, Earth Planet. Sc. Lett., 325–326, 93–99, doi:10.1016/j.epsl.2011.12.022, 2012. 1442, 1451
Huber, C., Beyerle, U., Leuenberger, M., Schwander, J., Kipfer, R., Spahni, R., Severinghaus, J. P., and Weiler, K.: Evidence for molecular size dependent gas fractionation in firn air derived from noble gases, oxygen, and nitrogen measurements, Earth Planet. Sc. Lett., 243, 61–73, doi:10.1016/j.epsl.2005.12.036, 2006. 1441
Hutterli, M. A., Schneebeli, M., Freitag, J., Kipfstuhl, J., and Rothlisberger, R.: Impact of local insolation on snow metamorphism and ice core records, in: Physics of Ice Core Records II, edited by: Hondoh, T., Hokkaido University Press, 223–232, 2010. 1442, 1450, 1451
Imbrie, J. and Imbrie, J. Z.: Modeling the climatic response to orbital variations, Science, 207, 943–953, doi:10.1126/science.207.4434.943, 1980. 1440
Jouzel, J., Waelbroeck, C., Malaize, B., Bender, M., Petit, J., Stievenard, M., Barkov, N., Barnola, J., King, T., Kotlyakov, V., Lipenkov, V., Lorius, C., Raynaud, D., Ritz, C., and Sowers, T.: Climatic interpretation of the recently extended Vostok ice records, Clim. Dynam., 12, 513–521, doi:10.1007/BF00207935, 1996. 1440
Jouzel, J., Hoffmann, G., Parrenin, F., and Waelbroeck, C.: Atmospheric oxygen 18 and sea-level changes, Quaternary Sci. Rev., 21, 307–314, doi:10.1016/S0277-3791(01)00106-8, 2002. 1440
Jouzel, J., Masson-Delmotte, V., Cattani, O., Dreyfus, G., Falourd, S., Hoffmann, G., Minster, B., Nouet, J., Barnola, J. M., Chappellaz, J., Fischer, H., Gallet, J. C., Johnsen, S., Leuenberger, M., Loulergue, L., Luethi, D., Oerter, H., Parrenin, F., Raisbeck, G., Raynaud, D., Schilt, A., Schwander, J., Selmo, E., Souchez, R., Spahni, R., Stauffer, B., Steffensen, J. P., Stenni, B., Stocker, T. F., Tison, J. L., Werner, M., and Wolff, E. W.: Orbital and millennial Antarctic climate variability over the past 800 000 years, Science, 317, 793, doi:10.1126/science.1141038, 2007. 1439, 1469, 1472
Kawamura, K., Parrenin, F., Lisiecki, L., Uemura, R., Vimeux, F., Severinghaus, J. P., Hutterli, M. A., Nakazawa, T., Aoki, S., Jouzel, J., Raymo, M. E., Matsumoto, K., Nakata, H.,

CPD
11, 1437–1477, 2015

Motoyama, H., Fujita, S., Goto-Azuma, K., Fujii, Y., and Watanabe, O.: Northern Hemisphere forcing of climatic cycles in Antarctica over the past 360 000 years, Nature, 448, 912–916, doi:10.1038/nature06015, 2007. 1441, 1442, 1445, 1446, 1448, 1449, 1468, 1472

Lambert, F., Delmonte, B., Petit, J. R., Bigler, M., Kaufmann, P. R., Hutterli, M. A., Stocker, T. F., Ruth, U., Steffensen, J. P., and Maggi, V.: Dust-climate couplings over the past 800 000 years from the EPICA Dome C ice core, Nature, 452, 616–619, doi:10.1038/nature06763, 2008. 1446, 1451

Landais, A., Caillon, N., Severinghaus, J., Jouzel, J., and Masson- Delmotte, V.: Analyses isotopiques à haute précision de l'air piégé dans les glaces polaires pour la quantification des variations rapides de température: méthodes et limites, Notes des activités instrumentales de l'IPSL, 39, 2003. 1443, 1444

Landais, A., Masson-Delmotte, V., Combourieu Nebout, N., Jouzel, J., Blunier, T., Leuenberger, M., Dahl-Jensen, D., and Johnsen, S.: Millenial scale variations of the isotopic composition of atmospheric oxygen over Marine Isotopic Stage 4, Earth Planet. Sc. Lett., 258, 101–113, doi:10.1016/j.epsl.2007.03.027, 2007. 1440, 1455

Landais, A., Dreyfus, G., Capron, E., Masson-Delmotte, V., Sanchez-Goñi, M., Desprat, S., Hoffmann, G., Jouzel, J., Leuenberger, M., and Johnsen, S.: What drives the millennial and orbital variations of $\delta^{18}O_{atm}$?, Quaternary Sci. Rev., 29, 235–246, doi:10.1016/j.quascirev.2009.07.005, 2010. 1440, 1455

Landais, A., Dreyfus, G., Capron, E., Pol, K., Loutre, M. F., Raynaud, D., Lipenkov, V. Y., Arnaud, L., Masson-Delmotte, V., Paillard, D., Jouzel, J., and Leuenberger, M.: Towards orbital dating of the EPICA Dome C ice core using $\delta O_2/N_2$, Clim. Past, 8, 191–203, doi:10.5194/cp-8-191-2012, 2012. 1441, 1442, 1443, 1445, 1446, 1449, 1453, 1458, 1468, 1469, 1475

Landais, A., Dreyfus, G., Capron, E., Jouzel, J., Masson-Delmotte, V., Roche, D., Prie, F., Caillon, N., Chappellaz, J., Leuenberger, M., Lourantou, A., Parrenin, F., Raynaud, D., and Teste, G.: Two-phase change in CO_2, Antarctic temperature and global climate during Termination II, Nat. Geosci., 6, 1062–1065, doi:10.1038/ngeo1985, 2013. 1440, 1443, 1445, 1452, 1455, 1469, 1472

Laskar, J., Robutel, P., Joutel, F., Gastineau, M., Correia, A. C. M., and Levrard, B.: A long-term numerical solution for the insolation quantities of the Earth, Astron. Astrophys., 428, 261–285, doi:10.1051/0004-6361:20041335, 2004. 1469

CPD
11, 1437–1477, 2015

Lefebvre, E., Arnaud, L., Ekaykin, A., Lipenkov, V., Picard, G., and Petit, J.-R.: Snow temperature measurements at Vostok station from an autonomous recording system (TAUTO): preliminary results from the first year operation, Ice and Snow, 4, 138–145, 2012. 1449, 1468

Lemieux-Dudon, B., Blayo, E., Petit, J.-R., Waelbroeck, C., Svensson, A., Ritz, C., Barnola, J.-M., Narcisi, B. M., and Parrenin, F.: Consistent dating for Antarctic and Greenland ice cores, Quaternary Sci. Rev., 29, 8–20, doi:10.1016/j.quascirev.2009.11.010, 2010. 1439

Leuenberger, M. C.: Modeling the signal transfer of seawater $\delta^{18}O$ to the $\delta^{18}O$ of atmospheric oxygen using a diagnostic box model for the terrestrial and marine biosphere, J. Geophys. Res., 102, 26841–26850, doi:10.1029/97JC00160, 1997. 1440

Lipenkov, V. Y., Raynaud, D., Loutre, M. F., and Duval, P.: On the potential of coupling air content and O_2/N_2 from trapped air for establishing an ice core chronology tuned on local insolation, Quaternary Sci. Rev., 30, 3280–3289, doi:10.1016/j.quascirev.2011.07.013, 2011. 1441, 1442

Loulergue, L., Schilt, A., Spahni, R., Masson-Delmotte, V., Blunier, T., Lemieux, B., Barnola, J.-M., Raynaud, D., Stocker, T. F., and Chappellaz, J.: Orbital and millennial-scale features of atmospheric CH_4 over the past 800,000 years, Nature, 453, 383–386, doi:10.1038/nature06950, 2008. 1439

Lüthi, D., Le Floch, M., Bereiter, B., Blunier, T., Barnola, J.-M., Siegenthaler, U., Raynaud, D., Jouzel, J., Fischer, H., Kawamura, K., and Stocker, T. F.: High-resolution carbon dioxide concentration record 650 000–800 000 years before present, Nature, 453, 379–382, doi:10.1038/nature06949, 2008. 1439

Malaizé, B., Paillard, D., Jouzel, J., and Raynaud, D.: The Dole effect over the last two glacial-interglacial cycles, J. Geophys. Res., 104, 14199–14208, doi:10.1029/1999JD900116, 1999. 1440

Marzin, C., Kallel, N., Kageyama, M., Duplessy, J.-C., and Braconnot, P.: Glacial fluctuations of the Indian monsoon and their relationship with North Atlantic climate: new data and modelling experiments, Clim. Past, 9, 2135–2151, doi:10.5194/cp-9-2135-2013, 2013. 1455

Masson-Delmotte, V., Stenni, B., Pol, K., Braconnot, P., Cattani, O., Falourd, S., Kageyama, M., Jouzel, J., Landais, A., Minster, B., Barnola, J. M., Chappellaz, J., Krinner, G., Johnsen, S., Röthlisberger, R., Hansen, J., Mikolajewicz, U., and Otto-Bliesner, B.: EPICA Dome C record of glacial and interglacial intensities, Quaternary Sci. Rev., 29, 113–128, doi:10.1016/j.quascirev.2009.09.030, 2010. 1446

CPD
11, 1437–1477, 2015

Masson-Delmotte, V., Buiron, D., Ekaykin, A., Frezzotti, M., Gallée, H., Jouzel, J., Krinner, G., Landais, A., Motoyama, H., Oerter, H., Pol, K., Pollard, D., Ritz, C., Schlosser, E., Sime, L. C., Sodemann, H., Stenni, B., Uemura, R., and Vimeux, F.: A comparison of the present and last interglacial periods in six Antarctic ice cores, Clim. Past, 7, 397–423, doi:10.5194/cp-7-397-2011, 2011. 1447, 1468

Meese, D. A., Gow, A. J., Grootes, P., Stuiver, M., Mayewski, P. A., Zielinski, G. A., Ram, M., Taylor, K. C., and Waddington, E. D.: The accumulation record from the GISP2 core as an indicator of climate change throughout the Holocene, Science, 266, 1680–1682, doi:10.1126/science.266.5191.1680, 1994. 1452

Paillard, D., Labeyrie, L., and Yiou, P.: Macintosh Program performs time-series analysis, EOS T. Am. Geophys. Un., 77, 379–379, doi:10.1029/96EO00259, 1996. 1469, 1471

Parrenin, F., Jouzel, J., Waelbroeck, C., Ritz, C., and Barnola, J.-M.: Dating the Vostok ice core by an inverse method, J. Geophys. Res., 106, 31837–31852, doi:10.1029/2001JD900245, 2001. 1439

Parrenin, F., Rémy, F., Ritz, C., Siegert, M. J., and Jouzel, J.: New modeling of the Vostok ice flow line and implication for the glaciological chronology of the Vostok ice core, J. Geophys. Res.-Atmos., 109, D20102, doi:10.1029/2004JD004561, 2004. 1439, 1452

Parrenin, F., Barnola, J.-M., Beer, J., Blunier, T., Castellano, E., Chappellaz, J., Dreyfus, G., Fischer, H., Fujita, S., Jouzel, J., Kawamura, K., Lemieux-Dudon, B., Loulergue, L., Masson-Delmotte, V., Narcisi, B., Petit, J.-R., Raisbeck, G., Raynaud, D., Ruth, U., Schwander, J., Severi, M., Spahni, R., Steffensen, J. P., Svensson, A., Udisti, R., Waelbroeck, C., and Wolff, E.: The EDC3 chronology for the EPICA Dome C ice core, Clim. Past, 3, 485–497, doi:10.5194/cp-3-485-2007, 2007. 1439, 1440, 1452, 1459

Petit, J. R., Jouzel, J., Raynaud, D., Barkov, N. I., Barnola, J.-M., Basile, I., Bender, M., Chappellaz, J., Davis, M., Delaygue, G., Delmotte, M., Kotlyakov, V. M., Legrand, M., Lipenkov, V. Y., Lorius, C., Pépin, L., Ritz, C., Saltzman, E., and Stievenard, M.: Climate and atmospheric history of the past 420 000 years from the Vostok ice core, Antarctica, Nature, 399, 429–436, doi:10.1038/20859, 1999. 1440, 1442, 1445, 1451, 1452, 1472

Picard, G., Domine, F., Krinner, G., Arnaud, L., and Lefebvre, E.: Inhibition of the positive snow-albedo feedback by precipitation in interior Antarctica, Nat. Clim. Change, 2, 795–798, doi:10.1038/nclimate1590, 2012. 1441, 1450

Raynaud, D., Lipenkov, V., Lemieux-Dudon, B., Duval, P., Loutre, M.-F., and Lhomme, N.: The local insolation signature of air content in Antarctic ice. A new step toward an absolute dating

CPD
11, 1437–1477, 2015

of ice records, Earth Planet. Sc. Lett., 261, 337–349, doi:10.1016/j.epsl.2007.06.025, 2007. 1441
Schaaf, C. B., Wang, Z., and Strahler, A. H.: Commentary on Wang and Zender – MODIS snow albedo bias at high solar zenith angles relative to theory and to in situ observations in Greenland, Remote Sens. Environ., 115, 1296–1300, doi:10.1016/j.rse.2011.01.002, 2011. 1450
Severinghaus, J. P. and Battle, M. O.: Fractionation of gases in polar ice during bubble close-off: new constraints from firn air Ne, Kr and Xe observations, Earth Planet. Sc. Lett., 244, 474–500, doi:10.1016/j.epsl.2006.01.032, 2006. 1441
Severinghaus, J. P., Grachev, A., and Battle, M.: Thermal fractionation of air in polar firn by seasonal temperature gradients, Geochem. Geophy. Geosy., 2, 2000GC000146, doi:10.1029/2000GC000146, 2001. 1444
Severinghaus, J. P., Beaudette, R., Headly, M. A., Taylor, K., and Brook, E. J.: Oxygen-18 of O_2 records the impact of abrupt climate change on the terrestrial biosphere, Science, 324, 1431, doi:10.1126/science.1169473, 2009. 1440, 1455
Shackleton, N. J., Hall, M. A., and Vincent, E.: Phase relationships between millennial-scale events 64 000–24 000 years ago, Paleoceanography, 15, 565–569, doi:10.1029/2000PA000513, 2000. 1440
Sime, L. C., Wolff, E. W., Oliver, K. I. C., and Tindall, J. C.: Evidence for warmer interglacials in East Antarctic ice cores, Nature, 462, 342–345, doi:10.1038/nature08564, 2009. 1447
Sowers, T., Bender, M., and Raynaud, D.: Elemental and isotopic composition of occluded O_2 and N_2 in polar ice, J. Geophys. Res., 94, 5137–5150, doi:10.1029/JD094iD04p05137, 1989. 1443
Spahni, R., Chappellaz, J., Stocker, T. F., Loulergue, L., Hausammann, G., Kawamura, K., Flückiger, J., Schwander, J., Raynaud, D., Masson-Delmotte, V., and Jouzel, J.: Atmospheric methane and nitrous oxide of the late pleistocene from Antarctic ice cores, Science, 310, 1317–1321, doi:10.1126/science.1120132, 2005. 1439
Stenni, B., Masson-Delmotte, V., Selmo, E., Oerter, H., Meyer, H., Röthlisberger, R., Jouzel, J., Cattani, O., Falourd, S., Fischer, H., Hoffmann, G., Iacumin, P., Johnsen, S. J., Minster, B., and Udisti, R.: The deuterium excess records of EPICA Dome C and Dronning Maud Land ice cores (East Antarctica), Quaternary Sci. Rev., 29, 146–159, doi:10.1016/j.quascirev.2009.10.009, 2010. 1447

CPD
11, 1437–1477, 2015

Suwa, M. and Bender, M. L.: O_2/N_2 ratios of occluded air in the GISP2 ice core, J. Geophys. Res.-Atmos., 113, D11119, doi:10.1029/2007JD009589, 2008a. 1448
Suwa, M. and Bender, M. L.: Chronology of the Vostok ice core constrained by O_2/N_2 ratios of occluded air, and its implication for the Vostok climate records, Quaternary Sci. Rev., 27, 1093–1106, doi:10.1016/j.quascirev.2008.02.017, 2008b. 1442, 1472
Svensson, A., Andersen, K. K., Bigler, M., Clausen, H. B., Dahl-Jensen, D., Davies, S. M., Johnsen, S. J., Muscheler, R., Parrenin, F., Rasmussen, S. O., Röthlisberger, R., Seierstad, I., Steffensen, J. P., and Vinther, B. M.: A 60 000 year Greenland stratigraphic ice core chronology, Clim. Past, 4, 47–57, doi:10.5194/cp-4-47-2008, 2008. 1439
Town, M. S., Waddington, E. D., Walden, V. P., and Warren, S. G.: Temperatures, heating rates and vapour pressures in near-surface snow at the South Pole, J. Glaciol., 54, 487–498, doi:10.3189/002214308785837075, 2008. 1441
Uemura, R., Masson-Delmotte, V., Jouzel, J., Landais, A., Motoyama, H., and Stenni, B.: Ranges of moisture-source temperature estimated from Antarctic ice cores stable isotope records over glacial–interglacial cycles, Clim. Past, 8, 1109–1125, doi:10.5194/cp-8-1109-2012, 2012. 1447
Veres, D., Bazin, L., Landais, A., Toyé Mahamadou Kele, H., Lemieux-Dudon, B., Parrenin, F., Martinerie, P., Blayo, E., Blunier, T., Capron, E., Chappellaz, J., Rasmussen, S. O., Severi, M., Svensson, A., Vinther, B., and Wolff, E. W.: The Antarctic ice core chronology (AICC2012): an optimized multi-parameter and multi-site dating approach for the last 120 thousand years, Clim. Past, 9, 1733–1748, doi:10.5194/cp-9-1733-2013, 2013. 1439, 1469, 1472
Waelbroeck, C., Frank, N., Jouzel, J., Parrenin, F., Masson-Delmotte, V., and Genty, D.: Transferring radiometric dating of the last interglacial sea level high stand to marine and ice core records, Earth Planet. Sc. Lett., 265, 183–194, doi:10.1016/j.epsl.2007.10.006, 2008. 1452
Wang, Y., Cheng, H., Edwards, R. L., Kong, X., Shao, X., Chen, S., Wu, J., Jiang, X., Wang, X., and An, Z.: Millennial- and orbital-scale changes in the East Asian monsoon over the past 224 000 years, Nature, 451, 1090–1093, doi:10.1038/nature06692, 2008. 1440, 1454, 1455
Wang, Y. J., Cheng, H., Edwards, R. L., An, Z. S., Wu, J. Y., Shen, C.-C., and Dorale, J. A.: A high-resolution absolute-dated late pleistocene monsoon record from Hulu cave, China, Science, 294, 2345–2348, doi:10.1126/science.1064618, 2001. 1455

CPD
11, 1437–1477, 2015

Table 1. Summary of present day local conditions at Vostok, Dome F and EDC (Masson-Delmotte et al., 2011; Kawamura et al., 2007; Landais et al., 2012; Lefebvre et al., 2012, this study).

Site	Lat. Long.	Elevation (m a.s.l.)	Nb of days after 21 December for max temp.	Mean albedo	Accu. rate (cm weq yr^{-1})	Mean annual temp. (°C)	10 m wind speed (m s^{-1})
Vostok	78°28′ S 106°48′ E	3488	10	0.83	2.15	−55.3	4.2
Dome F	77° 19′ S 39°40′ E	3810	0	0.80	2.3	−57.0	2.9
EDC	75°06′ S 123°21′ E	3233	5–20	0.83	∼ 2.5	−54.5	5.4

CPD
11, 1437–1477, 2015

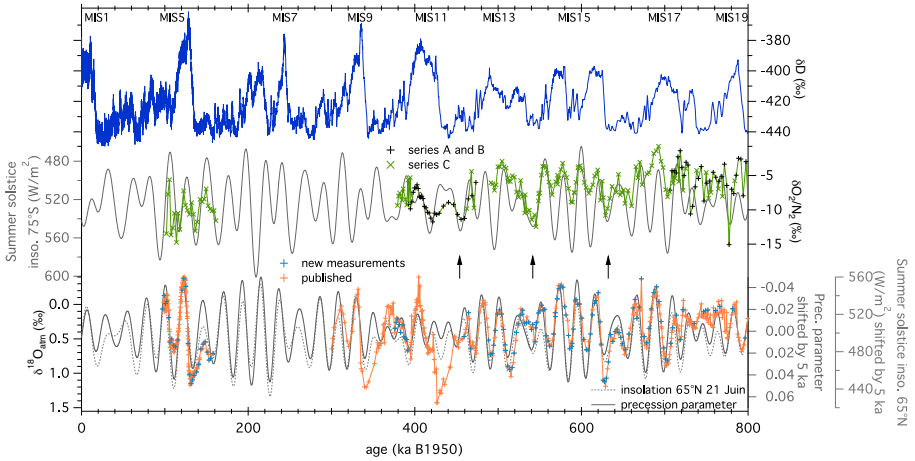

Figure 1. Top: EDC ice core record of water stable isotopes (δD, Jouzel et al., 2007). Middle: EDC record of $\delta O_2/N_2$ (black: Landais et al., 2012, green: this study) and local summer solstice insolation (grey, reversed axis). Bottom: EDC record of $\delta^{18}O_{atm}$ (reversed vertical scale) (orange: Dreyfus et al., 2007, 2008; Landais et al., 2013, blue: this study), precession parameter (grey, reversed axis) and 65° N summer solstice insolation (dashed grey) both shifted by 5 ka. All EDC records are presented on the AICC2012 chronology (Bazin et al., 2013; Veres et al., 2013). The orbital parameters are calculated using the Laskar et al. (2004) solution, with the Analyseries software (Paillard et al., 1996). Arrows mark the position of $\delta O_2/N_2$ minima characterizing the 100 ka periodicity.

CPD
11, 1437–1477, 2015

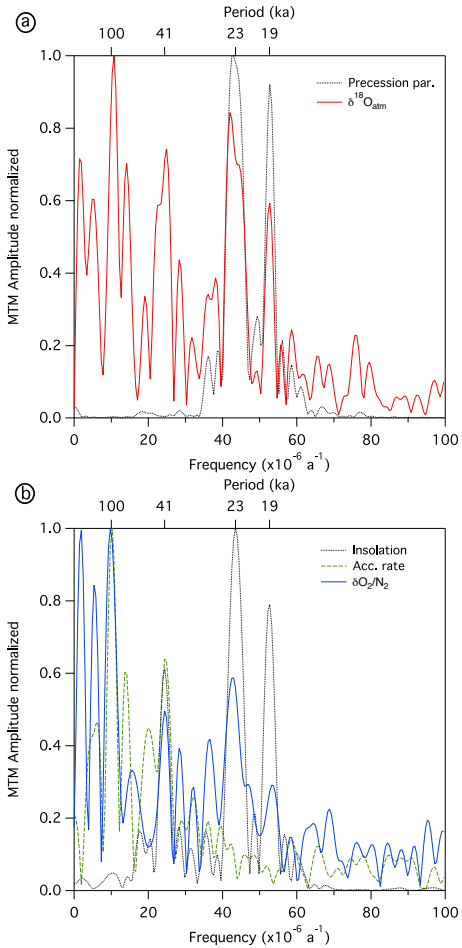

CPD
11, 1437–1477, 2015

Orbital forcing and air isotopic composition in Antarctic ice cores

L. Bazin et al.

Figure 2. Spectral analysis using the Multi–Taper Method with an interpolation step of 1 ka, obtained with Analyseries (Paillard et al., 1996). Amplitudes are normalized by the maximum value of each serie. **(a)** $\delta^{18}O_{atm}$ between 300–800 ka (red) presented with the precession parameter (grey). **(b)** $\delta O_2/N_2$ between 380–800 ka (blue) presented with local summer solstice insolation (grey) and AICC2012 accumulation rate (dashed green). Periods corresponding to significant peaks (F test > 90 %) are indicated on the upper horizontal axis.

CPD
11, 1437–1477, 2015

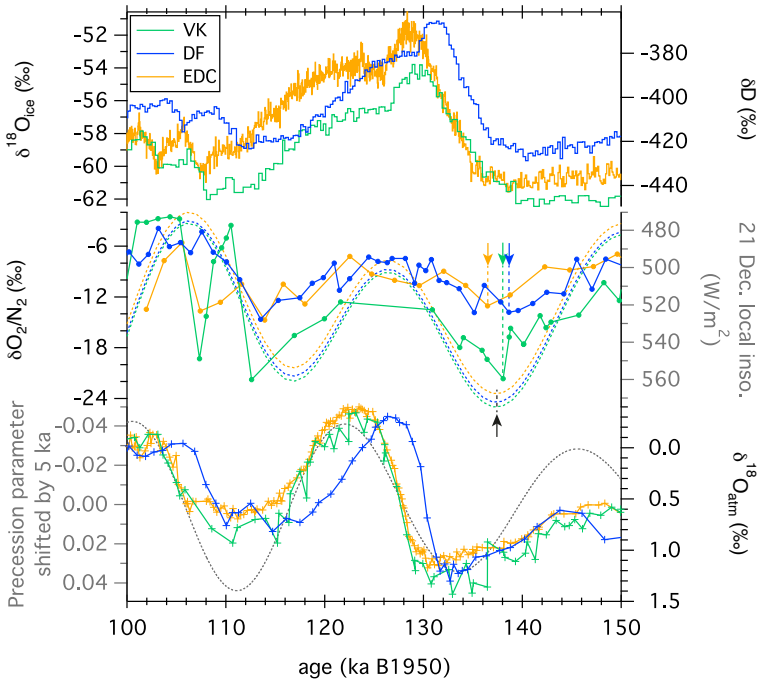

Figure 3. Inter-comparison of Vostok (green), Dome F (blue) and EDC (yellow) data covering MIS 5. Vostok and EDC data are presented on AICC2012 (Bazin et al., 2013; Veres et al., 2013) and Dome F on the DFO-2006 chronology (Kawamura et al., 2007). Top: water isotopic composition (Vostok $\delta^{18}O_{ice}$: Petit et al. (1999), Dome F $\delta^{18}O_{ice}$: Kawamura et al. (2007), EDC δD: Jouzel et al., 2007). Middle: $\delta O_2/N_2$ records and local summer solstice insolation at each site (Suwa and Bender, 2008b; Kawamura et al., 2007, this study). Bottom: $\delta^{18}O_{atm}$ and precession parameter shifted by 5 ka (Suwa and Bender, 2008b; Kawamura et al., 2007; Landais et al., 2013, this study). The arrows mark the different position of insolation maxima (black) and $\delta O_2/N_2$ minima (respective colors) before Termination II.

CPD
11, 1437–1477, 2015

Orbital forcing and air isotopic composition in Antarctic ice cores

L. Bazin et al.

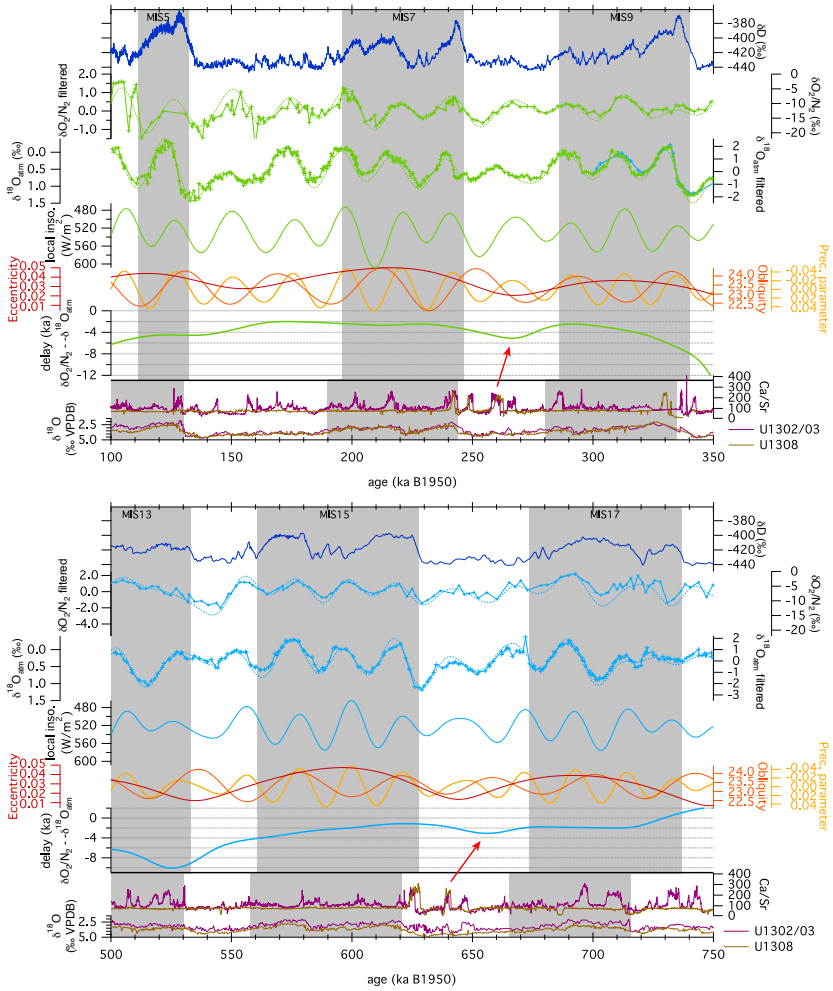

CPD
11, 1437–1477, 2015

Orbital forcing and air isotopic composition in Antarctic ice cores

L. Bazin et al.

Figure 4. Evolution of the phase delay between $\delta O_2/N_2$ and $\delta^{18}O_{atm}$ between 100–350 ka (top) and 500–750 ka (bottom). The Vostok data are represented in green and EDC data in light blue. The filtered data are first normalized (minus the mean and divided by the SD) and then filtered between 15–100 ka. From top to bottom: δD of EDC, $\delta^{18}O_{atm}$ on reversed axis (line with markers for raw data and dashed line for filtered data), $\delta O_2/N_2$ (line with markers for raw data and dashed line for filtered data), local summer solstice insolation of each sites (reversed axis), orbital parameters: precession (yellow, reversed axis), obliquity (orange) and eccentricity (red), phase delay calculated between $\delta O_2/N_2$ and $\delta^{18}O_{atm}$, Ca/Sr ratio of marine cores U1302/03 (purple) and U1308 (brown), $\delta^{18}O$ planktonic for U1302/03 (purple) and $\delta^{18}O$ benthic for U1308 (brown). Ice cores data are presented on the AICC2012 chronology. Marine data are presented on their respective core chronology. The grey rectangles mark the MIS intervals in both archives. The red arrows show the correspondence between the Heinrich-like events in the Ca/Sr records with the maximum delay of $\delta O_2/N_2$–$\delta^{18}O_{atm}$.

CPD
11, 1437–1477, 2015

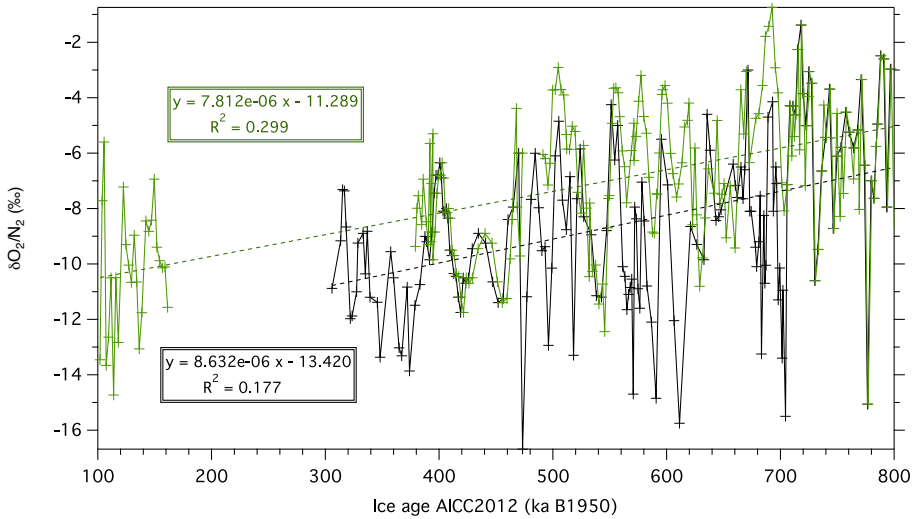

Figure A1. Comparison of the composite $\delta O_2/N_2$ record of Landais et al. (2012) (black) and the new $\delta O_2/N_2$ record measured on well-conserved ice (green). Both are presented on the AICC2012 chronology.

CPD
11, 1437–1477, 2015

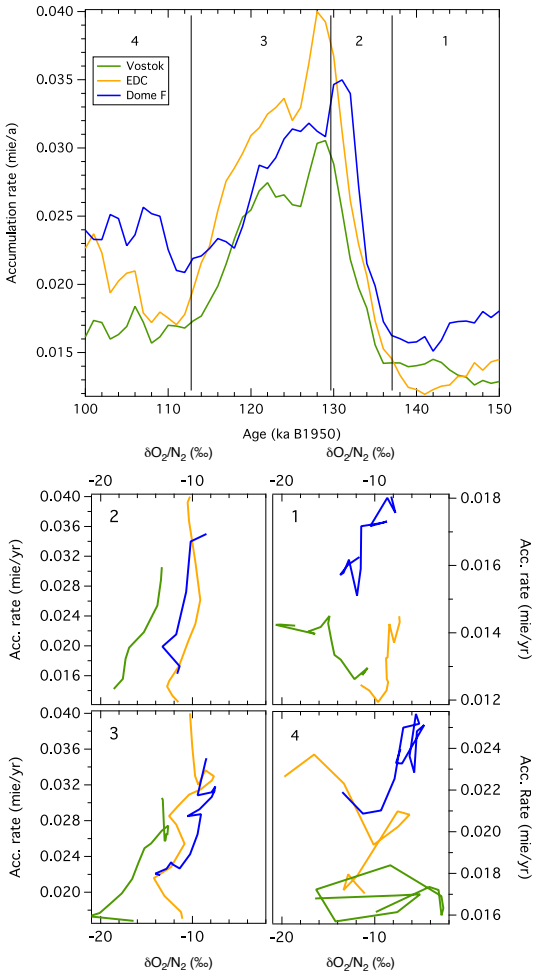

CPD
11, 1437–1477, 2015

Orbital forcing and air isotopic composition in Antarctic ice cores

L. Bazin et al.

Figure B1. (a) Comparison of accumulation rate of EDC, Vostok and Dome F. Vertical bars and numbers on top delimit approximately the four time intervals (numbered 1 to 4) for which accumulation rates are compared with $\delta O_2/N_2$ values for our three sites. **(b)** Plots of $\delta O_2/N_2$ vs. accumulation rate for the 4 periods delimited on **(a)**.

CPD
11, 1437–1477, 2015